Journal of Geodynamics 106 (2017) 1–11

Contents lists available at ScienceDirect

Journal of Geodynamics

journal homepage: http://www.elsevier.com/locate/jog

Crustal strain fields in the surrounding areas of the Ordos Block, central China, estimated by the least-squares collocation technique

Wei Qu[a,b], Zhong Lu[b,*], Ming Zhang[c], Qin Zhang[a], Qingliang Wang[d], Wu Zhu[a], Feifei Qu[a]

[a] College of Geology Engineering and Geomatics, Chang'an University, Xian Shaanxi, China
[b] Department of Earth Sciences, Southern Methodist University, Dallas, TX, USA
[c] Foundation Geomatics Technology Center, Yunnan Administration of Surveying, Mapping and Geoinformation, Kunming, Yunnan, China
[d] Second Monitoring Center, China Earthquake Administration, Xian Shaanxi, China

ARTICLE INFO

Article history:
Received 17 September 2016
Received in revised form
29 December 2016
Accepted 22 January 2017
Available online 27 January 2017

Keywords:
Surrounding areas of Ordos Block
Least-squares collocation technique (LSC)
GPS
Crustal strain rate fields
Tectonic geodynamics

ABSTRACT

The Ordos Block and its surrounding areas play a special role in the kinetic pattern of current tectonic deformation in mainland China (East Asia). In order to better understand the recent crustal deformation and geodynamics of this region, we use GPS velocities and employ the least-squares collocation (LSC) technique to estimate the distribution of the crustal strain rate fields. We calculate the principal components of strains, such as the maximum shear strains, the plane strain gradients and the principal axes of strains. The strain fields obtained in this paper can well portray crustal deformation in the region. Our results show that the relatively higher maximum shearing strain rates are mainly distributed over region surrounding the Ordos Block, indicating these periphery areas have intense crustal activities. Indeed, these periphery areas encompass major active tectonic belts (e.g., the western edge of the Qilian Fold System, the northeastern margin of the Tibetan Plateau and the Taihang Mountain) and active grabens (e.g., Yinchuan, Hetao, Shanxi and Weihe Grabens). Significant plane strain gradients concentrated over the periphery areas of the Ordos Block, indicating that these areas have more intense crustal activity and are more prone to earthquakes. The principle strain rates also show the strain rates for the periphery of the Ordos Block are higher than other regions. The highest strain rates are along the southwestern side of the Ordos Block, indicating that the eastward extrusion dynamics from the Tibetan Plateau may still be the main cause of tectonic deformation in this region. The extensional strains are present in most parts of the Yinchuan, Hetao and Shanxi Grabens. Finally, the characteristics of the strain fields predicted by the LSC technique are discussed, and some interesting tectonic deformation information can be found through further comparison with the strain results predicted by other methods The detailed results and findings obtained in this paper, could further help us better understand the recent active deformation and geodynamics in the surrounding areas of the Ordos Block.

1. Introduction

The surrounding areas of the Ordos Block in East Asia are ideal places for studying active tectonic deformation, because there are a series of intracontinental graben systems and a variety of fault and fold systems (Molnar and Deng, 1984; Molnar and Lyon-Caent, 1989; Deng et al., 2003; Liu et al., 2004; Yuan and Feng, 2010; Zhang et al., 2011a; Cheng et al., 2014; Liu et al., 2016; Cui et al., 2016). Because of the characteristics of the unique geological structure and spatially asymmetric seismicity, the surrounding areas of the Ordos Block have been studied as a hot topic for decades.

Recent geodetic, geologic and geophysical investigations have revealed various important aspects of this district. The horizontal crustal movements were described by GPS velocities (Yang et al., 2000; Dai et al., 2004; Chen et al., 2005; Guo et al., 2010; Zhang et al., 2011a; Qu et al., 2014a; Cui et al., 2016), and the vertical crustal movements were analyzed by leveling data (Hu et al., 2006a; Ta et al., 2014) and gravity measurements (Hu et al., 2006b). The crustal strain fields were studied by using the block model (Qu et al., 2014a) and the uniform deformation model (Cui et al., 2016) based on GPS observations. The characteristics of active faults and flexural fold structures were revealed by field investigations (Jiang et al.,

* Corresponding author.
E-mail address: zhonglu@smu.edu (Z. Lu).

http://dx.doi.org/10.1016/j.jog.2017.01.005
0264-3707/

2000a; Feng and Dai, 2004; Shi et al., 2008; Yang et al., 2013; Lin et al., 2015; Rao et al., 2015), and high-resolution remote-sensing imagery (Rao et al., 2014). The historical and current seismicity was reported in several studies (Jiang et al., 2000a; Song et al., 2012; Cheng et al., 2014; Liu et al., 2016). The tectonic stress fields were detected by fault slip data (Zhang et al., 2003), numerical simulations (Zhang et al., 2011b; Sun et al., 2015), and focal mechanism data (Wang et al., 2012; Li et al., 2015). The deep crustal structure and geophysical characteristics beneath the study area were probed by seismic wave data (Huang and Zhao, 2006; Chang et al., 2007; Tang et al., 2010; Ren et al., 2012; Li et al., 2014), and magnetic anomalies (Gao et al., 2015; Wang et al., 2015). In addition, some researchers also studied the recent ground fissure hazards of the study area (Myers and Gomez, 2010; Zhang et al., 2011b; Qu et al., 2014b).

Previous studies that applied different methods to investigate crustal deformation and tectonic activities in the surrounding areas of the Ordos Block have provided important references for the geodynamics of the region. Among above-mentioned technologies and methods, GPS technology has great advantages in studying active crustal deformation, particularly the crustal velocities of the region. Compared with the GPS velocity, the strain rate is independent of the frame of reference and can reveal local strain accumulation rates and their possible connections to seismic hazards (Ward, 1994; Riguzzi et al., 2012; Jiang and Liu, 2010; Wu et al., 2011, 2015). Strain rates of the region have been calculated by the block model (Qu et al., 2014a) and the uniform deformation model (Cui et al., 2016). These strain computation approaches have different applicability for different research purposes, but the strain results calculated by the two methods are useful for the inverse problem. However, sparseness and poor geometric distribution of GPS data as well as observation errors in GPS data may result in a biased strain field. Thus a more stable and robust technique should be considered to calculate crustal strain fields. The least-squares collocation (LSC) technique is a viable method to calculate the strain field by utilizing spatial interpolation and filtering based on a covariance function that describes the spatial correlations between any two observations. As the parameters of the covariance function are calculated using statistical methods, there is no subjective judgment involved in the calculation of crustal strain rate (Heiskanen and Moritz, 1967; Moritz, 1984; El-Fiky et al., 1997; Zhang et al., 1998a,b; Jiang et al., 2003; Wu et al., 2006; Jiang and Liu, 2010; Jiang et al., 2014; Wu et al., 2011, 2015).

In this paper, we delineate the crustal strain fields in the surrounding area of the Ordos Block using the high-precision GPS data from the Crustal Movement Observation Network of China (CMONOC). First, we apply the LSC technique to the GPS horizontal velocities to obtain the distribution of crustal strain fields in the region. Second, according to the strain results the recent active tectonic deformation characteristics of the region are revealed and the rationality of strain results is further explained based on the tectonic and geodynamics background. Finally, we discuss the characteristics of the strain rates predicted by the LSC technique, and also compare them with the strain results calculated by other methods.

2. Geological background

The Ordos Block and its surrounding areas is located in central China (Fig. 1). Geographically, this region represents the accommodation zone of differential movements of the following tectonic blocks: the northeastern margin of the Tibetan Plateau, the Qilian Fold System (a series of parallel NW trending mountain ranges) to the southwest; the Yinchuan basin and Alashan block to the northwest; the Hetao basin to the north (Yang et al., 2008); the Weihe

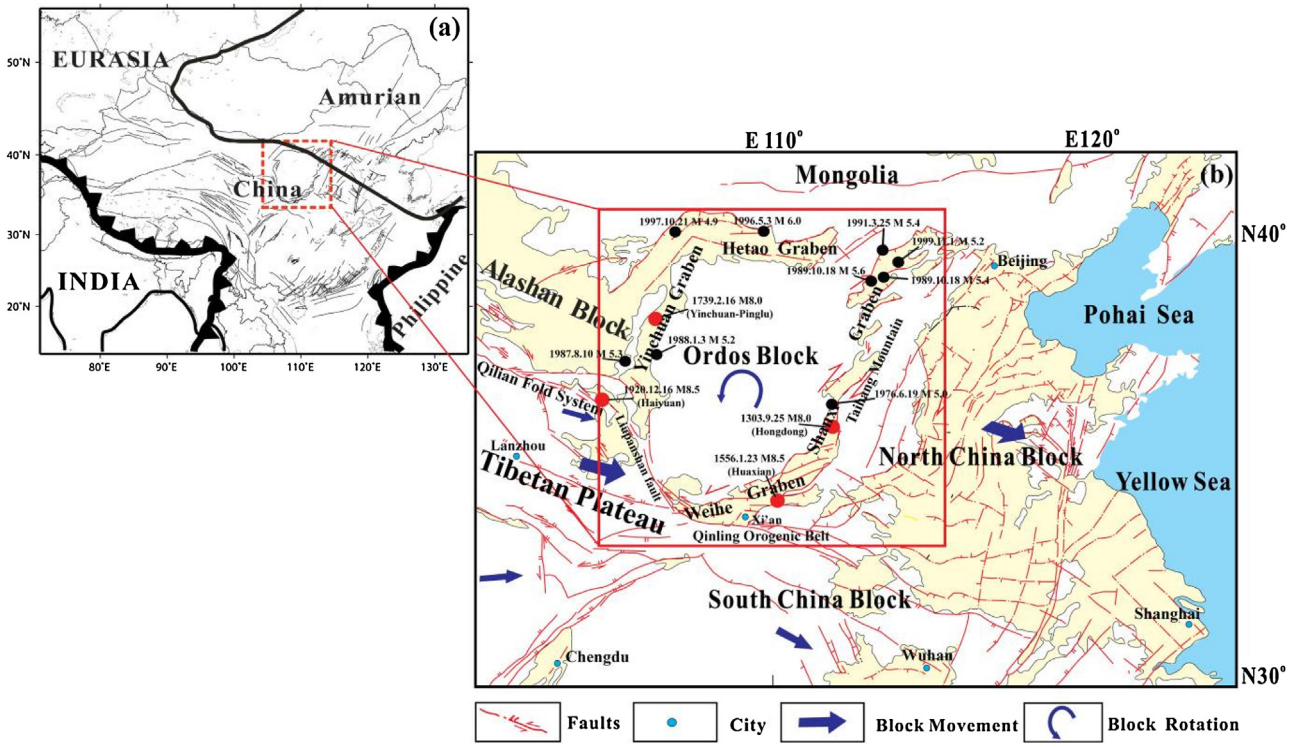

Fig. 1. Location of the region surrounding the Ordos Block in China. The red rectangular box outlines the study area. The thin navy blue arrow denotes the rotational motion characteristic of the Ordos Block while thick navy blue arrows represent the motion directions of major microplates in China. Light blue solid circle denote main cities in China, such as Beijing, Shanghai, Xi'an, Chengdu, Wuhan and Lanzhou. Red solid lines represent main faults in China (Zhang et al., 2005). The light blue regions represent the ocean in China, such as the Pohai Sea and the Yellow Sea. The light yellow regions represent the relatively low-lying regions. (For interpretation of the references to colour in this figure legend, the reader is referred to the web version of this article.)

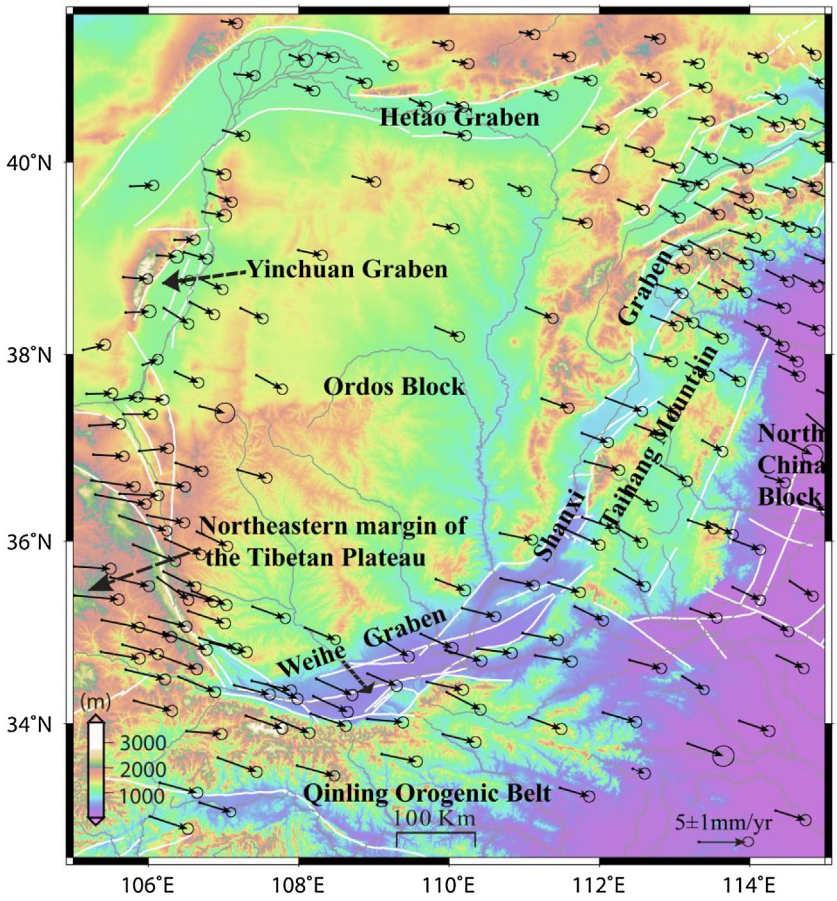

Fig. 2. GPS velocities in the surrounding areas of the Ordos Block for the period of 1999–2007. Solid arrows are observed GPS velocities with respect to the stable Eurasia plate based on ITRF2005 reference frame. Each arrow originates at the location of the station and points to its motion direction. The error ellipse represent the 95% confidence limit. The white stripes represent main faults over the region (Zhang et al., 2005).

Graben and Qinling Orogenic Belt to the south (Pan and Niu, 2011; Sun et al., 2014); the Shanxi Graben, Taihang Mountains and the western edge of the North China Block to the east (Zhang et al., 1998a,b; Jiang et al., 2000b; Tian et al., 2011) (Fig. 1). The Ordos Block and its surrounding areas play a special role in the kinetic pattern of current tectonic deformation.

Since the Cenozoic, a series of fault belts have developed around the stable Odors block (Deng and You, 1985; Xu, 2006). The NNW and NW reverse faults and extruded folds developed on the southwestern side of the Ordos Block due to the extrusion from Tibetan Plateau (e.g., the Haiyuan and Liupanshan faults). In contrast, normal faults are distributed on other margins of the Odors Block in the NNE or EW direction. Neotectonic movements frequently occurred in the sheared and strained tectonic zones around the Ordos Block (Bi et al., 2012). Large earthquakes frequently occurred on the periphery areas of the Ordos Block (Deng et al., 1996; Fan et al., 2003; Liu et al., 2016) including the 1920 M 8.5 Haiyuan earthquake on the southwestern side of the Ordos Block, the 1556 M 8.5 Huaxian earthquake on the eastern part of the Weihe Graben that destroyed 130 counties in 11 provinces and killed more than 830,000 people, the 1739 M 8.0 Yinchuan-Pingluo earthquake in the Yinchuan Graben, and the 1303 M 8.0 Hongdong earthquake in the Shanxi Graben (China Earthquake Administration (CEA), 1995; China Earthquake Administration (CEA), 1999; Gao et al., 2015; Rao et al., 2015). The seismicity over periphery areas of the Ordos Block in recent years is also active, and frequent earthquakes have brought huge destruction to the safety of human life and local economic development (Deng et al., 1996; Jiang et al., 2000a; Cheng et al., 2014; Liu et al., 2016).

3. GPS data and analysis

The GPS data in this paper are from CMONOC, which was built to investigate the crustal movement and deformation of mainland China. The GPS velocities used in the study were taken from Wang (2009), who processed the GPS data using the GAMIT/GLOBK software packages (King and Bock, 2000; Herring, 2002), based on the processing strategy used in Shen et al. (2000) and Gan et al. (2007). Station positions and velocities were estimated in the ITRF2005 reference frame (Altamimi et al., 2007) by using the QOCA software (http://gipsy.jpl.nasa.gov/qoca/). The QOCA modeling of the data was done through sequential Kalman filtering, allowing free rotation and translation for each daily solution and permitting certain parameters to have random walk style perturbations. (Dong et al., 1998, 2006; Shen et al., 2000; Gan et al., 2007). The GPS velocity fields can be further transformed into regional reference frames by applying constraints that minimize the motions within the stable interior of specific blocks. As the focus of this paper is on the analysis of the interior crustal deformation of the mainland China, the GPS velocity solutions were further transformed into a regional reference frame with respect to the Eurasia plate by applying constraints that minimize the motions at 11 IGS stations distributed within the stable plate interiors. Details on the GPS site selection are described in Qu et al. (2014a).

Fig. 2 shows the horizontal components of the GPS velocity vectors along with the 95% confidence error ellipses. These GPS velocity

vectors are representative of the recent secular deformation in surrounding areas of the Ordos Block. The GPS velocities indicate that the overall crustal movement of the study region is towards the southeast with respect to the Eurasia plate (Fig. 2). Relative to the Weihe basin and Qinling Orogenic Belt, the Hetao Graben has lower crustal movement velocities. The southwestern side of the Ordos Block and the Yinchuan Graben have larger crustal movement velocities than the Shanxi Graben and the western edge of the North China Block.

However, the spatial distribution of GPS velocity fields is just a direct reflection of crustal movement, while the crustal strain fields could further reflect the response of the internal mechanism of crustal deformation. Thus in this paper the above GPS horizontal velocities are further used to estimate the horizontal strain fields by the LSC technique which is discussed below.

4. Least-squares collocation (LSC) technique

The basic observation equation of the LSC technique can be briefly expressed as follows (Moritz, 1984; Jiang et al., 2001; Jiang and Liu, 2010; Wu et al., 2011):

$$V = B_Z\hat{Z} + G\hat{Y} - L \tag{1}$$

where Z represents the estimates of signal at any location either observed station or estimated position, B_Z is the coefficient matrix for the signal: identity matrix for observed points but a zero matrix for estimated points, G is a design matrix, $\hat{Y}$ is a vector of model parameters (non-random), L is vector of the observed values. According to Eq. (1), crustal movement can be described as a combination of the whole movement ($G\hat{Y}$), the deformation ($B_Z Z$) and the error (V). According to the theory of the indirect adjustment and matrix inversion (Yu and Lu, 1978; Wu et al., 2009), the solution of Eq. (1) can be obtained as follows (Wu et al., 2011):

$$\begin{cases} \hat{Y} = \left\{G^T(D_X + D_\Delta)^{-1}G\right\}^{-1}G^T(D_X + D_\Delta)^{-1}L \\ \hat{Z} = D_Z(D_X + D_\Delta)^{-1}(L - G\hat{Y}) \end{cases} \tag{2}$$

where D_X represents the covariance matrix of signals at the observed stations, D_Z is the covariance matrix of signals at all positions (including the observed stations and estimated positions), and D_Δ is the covariance matrix of observed values.

Eq. (2) is a theoretical formula of the LSC technique. To compute crustal movement using this equation, it is necessary to determine the characteristics of the covariance distribution in advance (Jiang et al., 2003). The most common way is to use empirical covariance function (ECF) to fit the covariance distribution. The Gaussian function ($C(d) = C(0)\exp\left\{-k^2d^2\right\}$ (Jiang and Liu, 2010; Wu et al., 2011, 2015) or the exponential function ($C(d) = C(0)\exp\left\{-kd\right\}$) (Jiang et al., 2014), has been taken as the ECF to calculate the covariance matrix in the analysis of crustal movement: where $C(0)$ and k are the constants estimated from a covariance plot of the data, d is the distance between the GPS stations, and $C(d)$ is the covariance value. Then D_Z and D_X in Eq. (2) are constructed from $C(d)$. Once the covariance functions are determined, it becomes possible to estimate the signal (e.g., horizontal GPS velocity fields) at estimated points in the study area (El-Fiky et al., 1997; Wu et al., 2009; Jiang and Liu, 2010). Further, the estimated velocities can be differentiated in space to calculate the strain rate components in latitude, longitude and shear directions ($\varepsilon_\phi, \varepsilon_\lambda, \gamma_{\lambda\phi}$) in the spherical coordinates based on the differential relationship between velocity and strain rate (Shi and Zhu, 2006; Fu and Huang, 2001; Jiang et al., 2003; Wu et al., 2009). Based on these strain rates components, the principal components of strain rates such as the maximum shear strain rate, the plane strain gradient, principal strain rates can be further calculated (Turcotte and Schubert, 1982; Zhang et al., 2013; Wu et al., 2015).

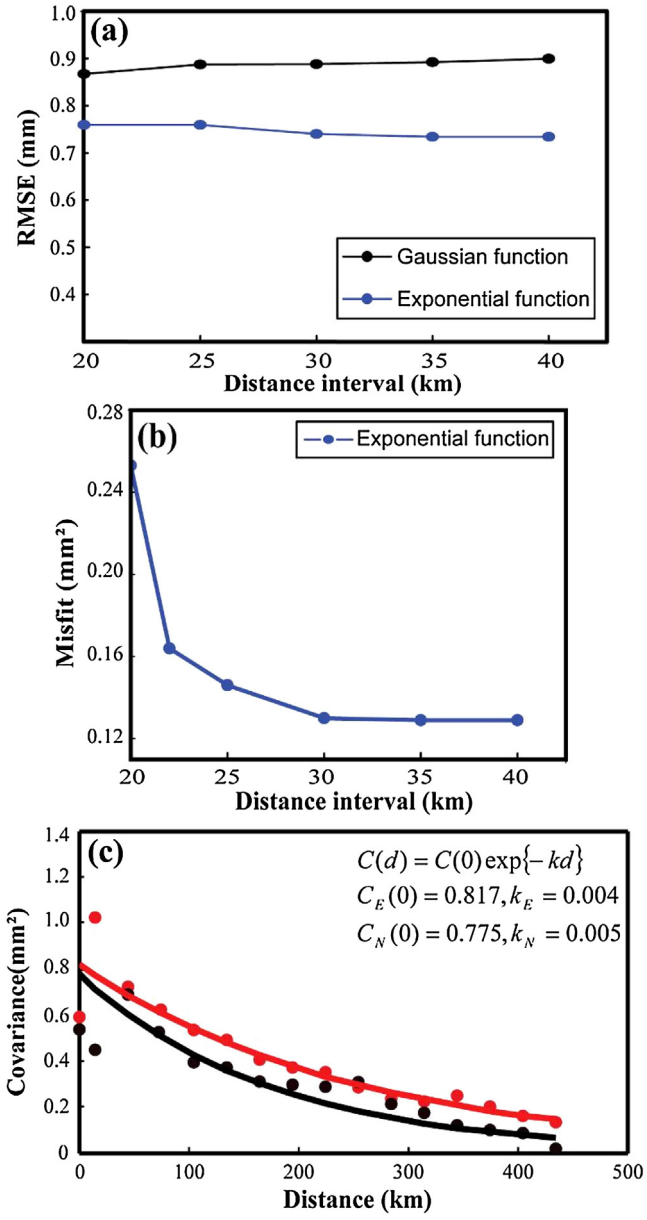

Fig. 3. (a) the fitness to the GPS observations using the Gaussian function, Hirvonen function and Exponential function, respectively, (b) the misfit to the statistics of variance and covariance using the exponential function with different statistical distance intervals, and (c) the statistics of variance and covariance and two empirical exponential covariance functions calculated from GPS velocity during 1999–2007. The red color denotes the E-W component of the GPS measurements. The black color represents the N-S component. (For interpretation of the references to colour in this figure legend, the reader is referred to the web version of this article.)

5. Strain results and analysis

5.1. Estimation of the crustal strain rates using LSC technique

Here, we employ the LSC technique to estimate the crustal strain rate field based on the GPS observations shown in Fig. 2. We use abovementioned ECFs (Gaussian and exponential functions) to construct the variance-covariance matrixes. Then the GPS velocities at observation stations can be predicted using the LSC technique. Fig. 3a shows the misfits to GPS observations from the two differ-

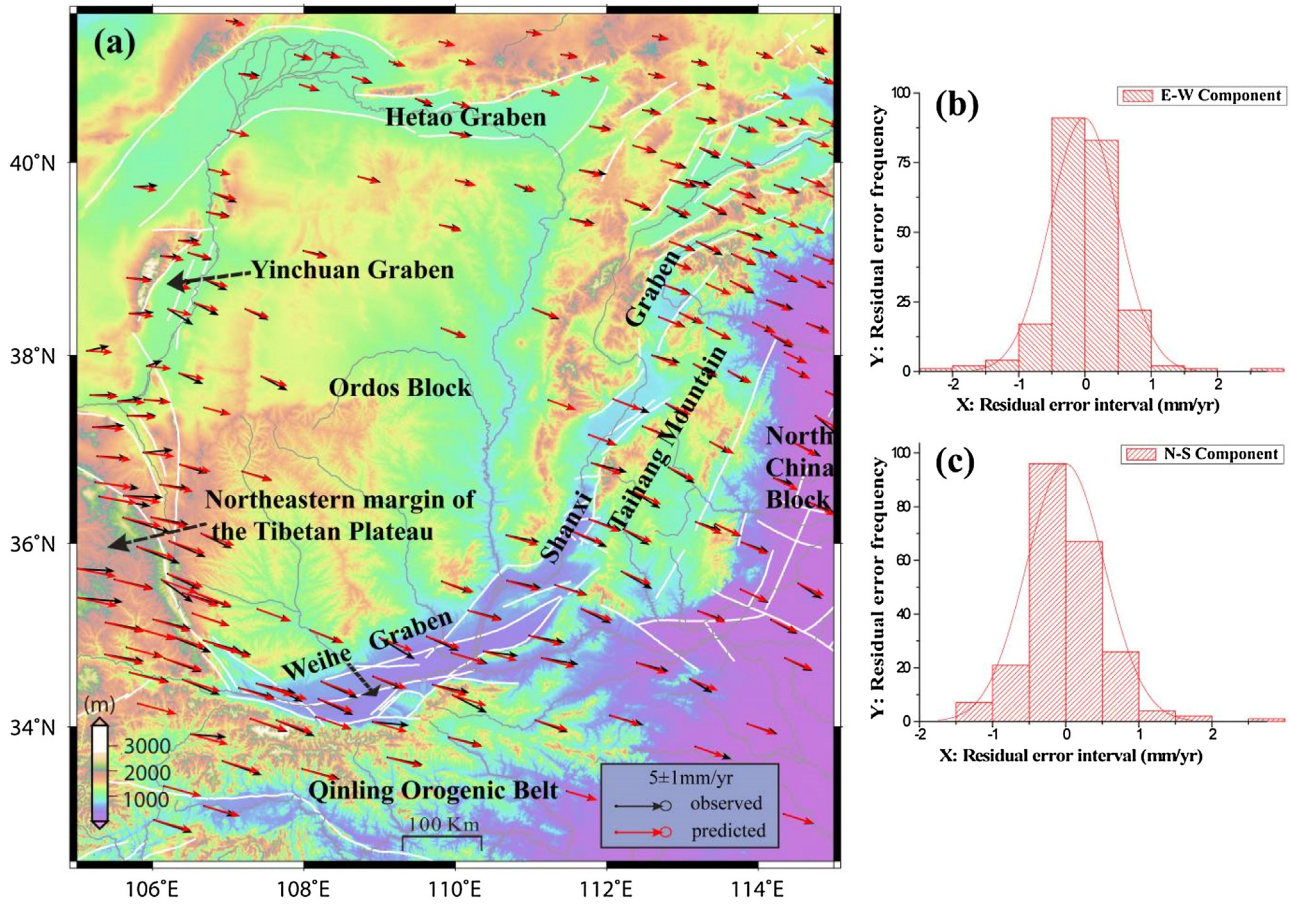

Fig. 4. (a) comparison of the observed GPS velocities (black arrows) and the predicted velocities (red arrows) based on LSC technique at each GPS station, (b) and (c) histograms of residuals between the observed and predicted velocities in the E-W and N-S components. (For interpretation of the references to colour in this figure legend, the reader is referred to the web version of this article.)

ent covariance functions at different statistical distance intervals. The minimum root-mean-square error (RMSE) is obtained by using the exponential function (Fig. 3a). Therefore, the exponential function is chosen as the local empirical covariance function of this study area. Additionally, in order to determine the better distance interval, we further calculate the misfits to the variances and covariances at different intervals using exponential function. The results (Fig. 3b) show that a trade-off point may appear at the distance interval of 30 km. So we take 30 km as the best distance interval to calculate the statistics of variance and covariance.

The final parameters of the covariance function (in exponential form) for E-W and N-S components of GPS velocity fields are shown in Fig. 3c (only selected values used to invert the empirical local covariance function are plotted in Fig. 3c). We can conclude that the correlation distance is approximately 400–500 km and the correlation distance of the E-W component is larger than that of the N-S component. The reliability of the estimated strain rates depends on the quality of the fit to the GPS velocity data, so we first analyze the characteristics of the residual errors between the observed and the LSC-predicted at GPS observation stations. Fig. 4a shows the comparison between the observed GPS velocities and the model-predictions based on LSC technique by using exponential function as the local empirical covariance function. The RMSE value is only 0.74 mm/yr. The histogram results (Fig. 4b and c) further show that the residual distribution satisfies the requirement for normality and lacks of bias.

5.2. Distribution of the crustal strain rates

Fig. 5 shows that the maximum shear strain rates are mainly along the periphery areas of the Ordos Block. The northeastern margin of the Tibetan Plateau, the western edge of the Qilian Fold System and the Yinchuan Graben over the southwestern and northwestern sides of the Ordos Block possess the highest value of the maximum shearing strain rate (about 1.6×10^{-8}/yr). Almost the whole Shanxi Graben, the central areas of the Taihang Mountain and the western edge of the North China Block over the eastern side of the Ordos Block have relative higher maximum shearing strain rate (about 1.2×10^{-8}/yr). Additionally, the middle and eastern edges of the Hetao Graben, the western and eastern areas of the Weihe Graben, the junction areas between the Qinling Orogen Belt and the North China Block also have higher maximum shearing strain rate.

The magnitude of the shear strain rate reflects the degree of the crust deformation; the higher the shear strain rate, the more severe the crustal activity. Furthermore, higher rates of strain accumulation generally should be associated with larger or more frequent earthquakes (Segall, 2010). Indeed, those areas holding higher maximum shearing strain rates correspond to tectonically active zones surrounding the Ordos Block, including the northeastern margin of the Tibetan Plateau, the western edge of the Qilian Fold System, Yinchuan, Hetao, Shanxi and Weihe Grabens. More importantly, strong historical and recent earthquakes frequently occurred in these areas (Fig. 1). The relatively higher maximum shearing strain

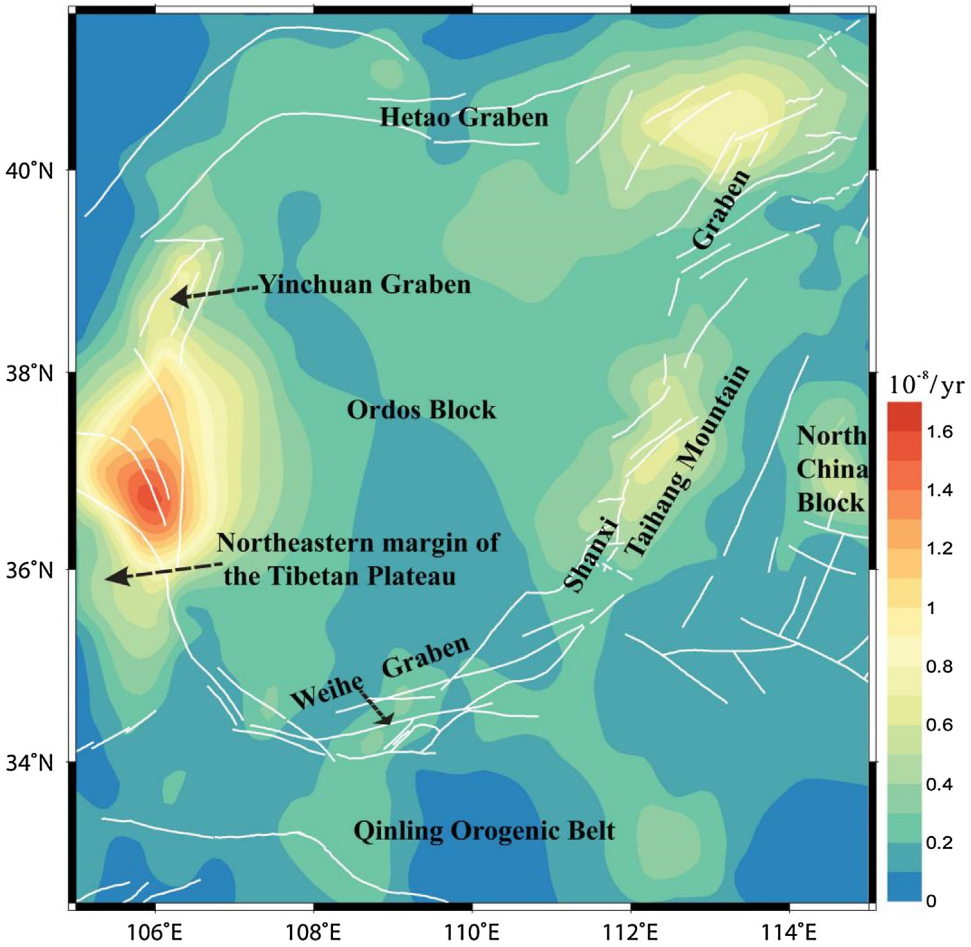

Fig. 5. The distribution characteristics of maximum shear strain rates of the areas surrounding the Ordos Block for 1999–2007 (unit:10^{-8}/yr).

rate appear in the Taihang Mountain and the western edge of the North China Block. This is also consistent with the geophysical and geological observations showing low velocities beneath the Taihang Mountains, the Shanxi Graben and the western edge of the North China Block (Chang et al., 2007). The lower seismic velocity is representative of weakness in the underlying crust. Geological observations have also suggested that the active deformation on the eastern side of the Ordos Block is localized mainly around the narrow Shanxi Graben (Wesnousky et al., 1984; State Seismological Bureau Research Group (SSBRG), 1988; Xu and Ma, 1992), and around the Taihang Mountains and the western edge of the North China Block (Ye et al., 1985; Tian et al., 1992). Additionally, higher maximum shearing strain rate appear in the junction areas between the Qinling Orogen belt and the North China Block, suggesting that these areas were formed in response to the collision between the South China Block and North China Block and this dynamic process may still be continuing (Meng and Zhang, 2000; Ratschbacher et al., 2003; Chen et al., 2015; Guo and Chen, 2016). The crustal activity is also intense and there has been a long historical record of earthquakes around this areas (Shaanxi Earthquake Information Network (SEIN), 2011).

Plane strain gradients describe the gradients of the areal dilatational strain that can portray the enhancement, range and the duration of the crustal stress. To certain extent, the distribution of plane strain gradient can reflect the characteristics of the differential motions among the tectonic block boundaries (Zhang et al., 2013). The region with high strain gradient indicates that the areal dilatational strain change significantly in space. The transition zone possessing large spatial variations in plane strain gradients indicates higher likelihood of strong earthquakes, which can used be for medium to long-term earthquake prediction in mainland China (Zhang et al., 2013).

Compared with the distribution of the maximum shear strain rates (Fig. 5), the transition zones of the high and low plane strain gradients concentrate on the periphery areas of the Ordos Block, such as along the southwestern side of the Ordos Block, the whole Yinchuan Grabens, most parts of the Hetao, Shanxi and Weihe Grabens, the central areas of the Taihang Mountain and the western edge of the North China Block, the junction areas between the Qinling Orogen belt and the North China Block (Fig. 6). These transition zones of the significant plane strain gradients indicate the strain accumulation in these areas reach the maximum and are therefore the dangerous areas where large earthquakes likely occur (Zhang et al., 2013). This feature is also consistent with the aggregation of the spatial distribution of earthquakes in this region (historical and recent earthquakes shown in Fig. 1) (China Earthquake Administration (CEA), 1995; China Earthquake Administration (CEA), 1999; Deng et al., 1996; Fan et al., 2003; Liu et al., 2016) (Fig. 7).

The compressional strain rates are in the nearly NE-SW direction and mainly along the southwestern side of the Ordos Block, accompanied by the extensional strain in the NW-SE direction. This feature may be formed if the eastward movement of the crustal material of the Tibetan Plateau encounters the associated resistance of the stable Alashan and Ordos Blocks (England and Houseman, 1986; Liu et al., 2007; Bai et al., 2010; White and Lister, 2012). Over the Yinchuan Graben, most parts mainly present extensional strain rates in the NW-SE direction, while local areas in the south

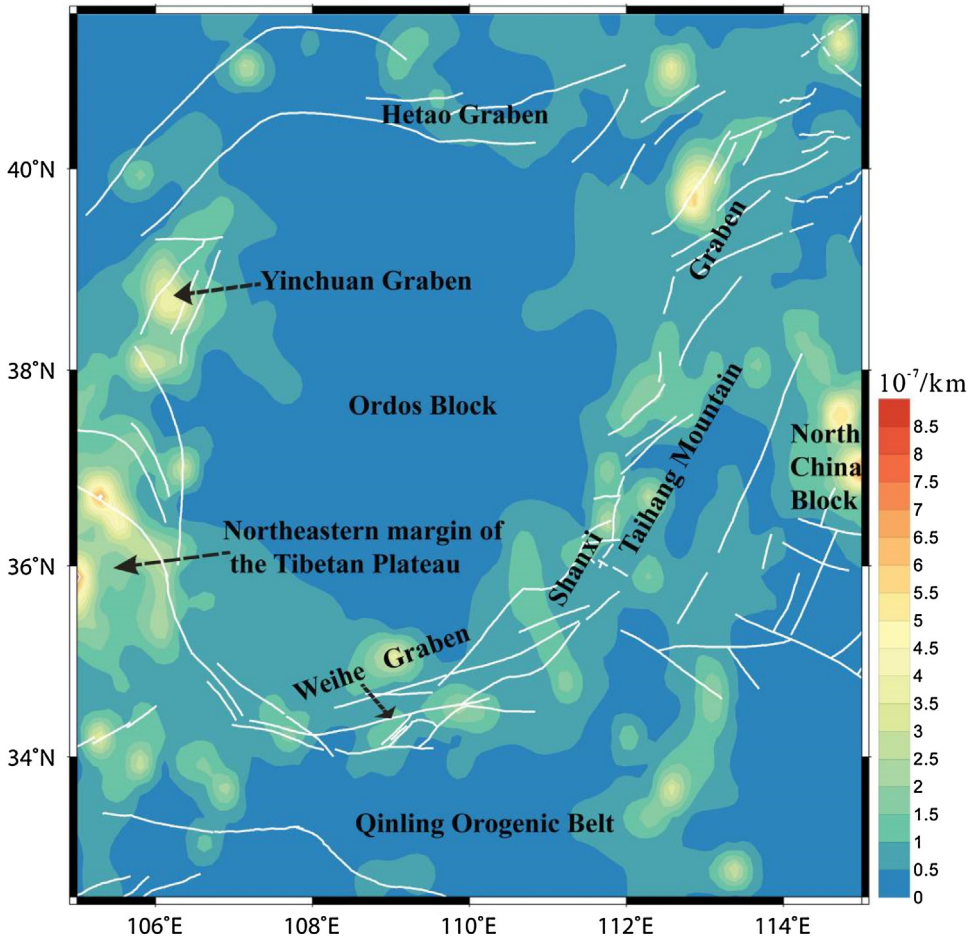

Fig. 6. The distribution characteristics of plane strain gradient of the areas surrounding the Ordos Block for 1999–2007 (unit:10^{-7}/km).

show compressional strain rates. The Hetao basin overall presents extensional strain rates in the NW-SE direction, especially in the middle-eastern parts. The northern Shanxi Graben presents significant extensional strain rates in the NW-SE direction and the central areas of the Shanxi Graben also have extensional strain rates. The western edge of the Shanxi Graben mainly presents extensional strain while the eastern edge compressional strain. The whole Shanxi Graben has characteristics of dextral tension, while the overall Weihe Graben shows characteristics of slightly left lateral compression. The junction areas between the Qinling Orogen and the North China Block present obviously compressional strain rates; this feature might be related to the evolving stress field of the Qinling Orogenic Belt formed in response to the collision between the North China Block and South China Block. This also may be the reason that the principle strain rate in the Weihe basin dose not possess significant extensional feature. Additionally, there are two higher strain rates zones: a higher compressional strain zone in the central Taihang Mountain, and a higher extensional strain zone over the central western of the North China Block (at coordinates about 37.2°N, 114.9°E). This phenomenon may also indicate that the crustal activities in these higher strain zones are significantly different from adjacent areas, as shown in Figs. 5 and 6.

6. Discussions

6.1. Characteristics of the strain rate fields predicted by LSC

We use the exponential function as the local empirical covariance function to carry out the LSC calculation over our study area. However, the misfit to GPS observations from the Gaussian function is relatively higher (average RMSE ~0.89 mm/yr) (Fig. 3a). It should be noted that the Gaussian function has been successfully used to fit the signal covariance in other regions in mainland China (Zhang et al., 1998a,b; Jiang et al., 2003; Wu et al., 2006; Jiang and Liu, 2010; Jin et al., 2012; Wu et al., 2011, 2015). Therefore, the choice of the empirical covariance function depends on the GPS observations in the specific study area.

Additionally, when we construct the empirical covariance function based on the GPS observations, the decay model of the covariance with the site spacing is not only related to the spatial distribution of the GPS observations, but also specific to the study region (Jiang and Liu, 2010). Therefore, the strain rates estimated from the covariance constructed by different decay models actually take into account the deformations in different frequency domain. For example, the maximum shear strain (plane strain gradient) rates in the surrounding areas of the Ordos Block have different scales from that the entire mainland China (GPS data during 1999–2007) (Zhang et al., 2013). These differences illustrate that the strain rates in this study can reflect more detailed local deformation. The maximum shear strain rates (the transition zones of the high and low plane strain gradients) mostly concentrate on the periphery areas of the Ordos Block. Most importantly, these periphery areas all possess the most intense crustal activity belts within the study area. We can see that the deformation information in relatively high frequency domain has been identified by using the LSC technique. On the other hand, the above analysis also indicates that the uniqueness of the strain field, which is not affected by the

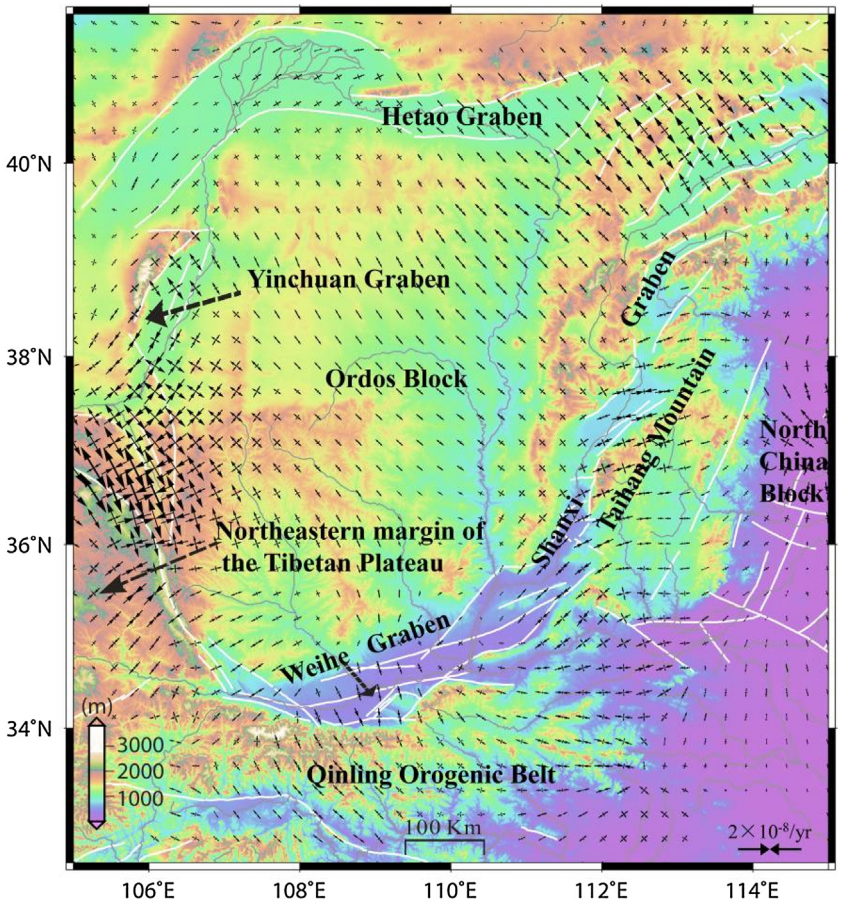

Fig. 7. The distribution characteristics of the principal strain rates of the areas surrounding the Ordos Block for 1999–2007 (unit:10^{-8}/yr).

reference frame, may be affected by the different spatial frequency domain and error filtering (Jiang and Liu, 2010).

6.2. Comparison with the strain results calculated by other methods

Previous studies on the Ordos and its surrounding areas were summarized in the introduction section. The latest study on the analysis of crustal strain fields was carried out by using the block model (Qu et al., 2014a) and the uniform deformation model (Cui et al., 2016).

Although the observation time of the GPS data in the study of Cui et al. (2016) does not overlap with this study, the crustal deformation should be consistent if there is no large tectonic event occurred in the region). Indeed, there was no big earthquake (ML > 5.5) occurred in this study area during the two observations, and the coseismic effects (e.g., 2001 Kokoxili M 8.1, 2008 Wenchuan M 8.0, 2010 Yushu M 7.1 and 2011 Japan M 9.0 earthquakes) have also been removed from the GPS velocity (Wang, 2009; Cui et al., 2016). In addition, in the study of Cui et al. (2016) the GPS velocity fields were also firstly estimated on grid points by using the LSC technique, then the strain results were calculated based on the linear functional relation between the velocity and the strain rate under the assumption that the medium is homogeneous and the strain is uniform between adjacent points (Zhang et al., 1998a,b). Therefore, it's useful to compare the strain results of Cui et al. (2016) with those from this study.

There are similar characteristics in the two studies, but also exist some differences. Both studies show that compressional strain rates in the nearly NE-SW direction are mainly along the southwestern side of the Ordos Block (accompanied by the extensional strain in the NW-SE direction). This feature may indicate that the eastward extrusion from the Tibetan Plateau may still be the main cause of tectonic deformation of the region (Wang et al., 2013). Most of the Yinchuan Graben mainly presents extensional strain in the NW-SE direction, the Hetao basin overall presents extensional strain in the NW-SE direction especially in the middle-eastern areas, the northern and central of the Shanxi Graben present extensional strain rates, the west edge of the Shanxi Graben mainly presents extensional strain and the east edge presents compressional strain. These similar characteristics from the two studies all reveal that the higher strain rates almost concentrate along the periphery of the Ordos Block, which is consistent with the recent dynamics background over the region (Bi et al., 2012). However, Cui et al. (2016) presented the compressional strain on the southwestern corner of the study area, and relative complex principle strain rates within the Weihe basin and Qinling Orogenic belt. It may indicate the tectonic stress field in this area has been modified after the 2008 Wenchuan M 8.0 and 2010 Yushu M 7.1 earthquakes. The direction of the extensional strain axis in the western edge of the Shanxi Graben has also changed, indicating the tectonic stress field in this area has been adjusted after the 2011 Japan M 9.0 earthquake.

It is difficult to compare the strain results calculated by the block model (Qu et al., 2014a) with the spatial distribution strains predicted by the LSC technique in this paper. Because the block model approach divides the study area into several blocks and computes the strain parameters for each block. The spatial distribution of the strain field is made of individual results from all blocks. The spatial distribution from the block model is a process of rejecting gross error and performing grid processing, which is not strictly continu-

ous processing and filtering and also can be affected by the density of observations and observation errors. However, the LSC technique is useful for estimating nonrandom parameters, signal with random attributes, and random errors. The LSC technique realizes the spatial interpolation and filtering based on a covariance function that describes the spatial correlations between any two points. But even so, the strain results calculated by the block model could well reflect the overall tectonic features of separated blocks (Qu et al., 2014a).

7. Conclusions

In this paper, we use the LSC technique to calculate the strain rate fields over the surrounding areas of the Ordos Block based on the high- precision GPS data from the CMONOC. The LSC technique is proved to be an effective method for obtaining the distribution of the strain rate field, which well portrays recent active crustal deformation and geodynamics in the region.

The relatively high maximum shearing strain rates are mainly along the periphery areas of the Ordos Block, such as the southwestern side of the Ordos Block (the northeastern margin of the Tibetan Plateau and the western edge of the Qilian Fold System), the whole Yinchuan Graben, the middle and eastern edge areas of the Hetao Graben, almost the whole Shanxi Graben, the central areas of the Taihang Mountain and the western edge of the North China Block, the western and eastern areas of the Weihe Graben, the junction areas between the Qinling Orogen Belt and the North China Block. These features indicate that these periphery areas hold intense crustal activities.

Compared with the distribution of the maximum shear strain rates, the distribution of the plane strain gradient could more clearly portray that the transition zones of the high and low values significantly concentrate on the periphery areas of the Ordos Block. This feature further indicates that these periphery areas have more intense crustal activity and are more prone to earthquakes.

The distribution of the principle strain rates also shows the strain rates for the periphery areas of the Ordos Block are higher than other regions. The compressional strain rates in the NE-SW direction are mainly along the southwestern side of the Ordos Block, the junction areas between the Qinling Orogen Belt and the North China Block. The highest strain rates are significant along the southwestern side of the Ordos Block, which indicates that the eastward extrusion dynamics from the Tibetan Plateau may still be the main cause of tectonic deformation (Wang et al., 2013). The extensional strain in the NW-SE direction are mainly presented in most parts of the Yinchuan, Hetao and Shanxi Grabens. The two sides of Shanxi Graben show distinct strain characteristics: the western side mainly presents extensional strain while the eastern side presents compressional strain. These features are consistent with the tectonic background of the region.

Through further comparing with the strain results calculated by other methods, we further find that the crustal tectonic deformation of the study area is temporally continuous, and some differences may indicate the tectonic stress field has been adjusted in local areas. The detailed results and findings obtained in this paper could further help us to better understanding the recent crustal deformations and geodynamics in the area surrounding the Ordos Block. It also should be pointed out that the GPS observations can provide accurate and large-scale information of the crustal movement, which reflects the present-day activity level of the crustal active deformation. However, the observation of nearly 8 years is still only a brief moment if compared with the geological time scales. Therefore, in order to further understand the evolution of geodynamics of the study area, our future work will continue the monitoring of crustal movement to obtain longer time-scale GPS observations, along with additional level monitoring and large-scale satellite observations.

Acknowledgements

The authors are grateful to surveyors who works hard in the areas surrounding the Ordos Block in tough environment to obtain GPS data. Thanks to Prof. M. Wang and researchers from the China Seismological Bureau's the Second High-tech Research Center for providing the high precision GPS horizontal data. This study was supported by the China Scholarship Fund of China Scholarship Council (CSC), also supported by Nature Science Fund of China (NSFC) (project Nos: 41674001, 41628401, 41604001, 41504005, 41202189, 41274004, 41274005), the Project Supported by Natural Science Basic Research Plan in Shaanxi Province of China (Program No. 2016JM4005), and China Postdoctoral Science Foundation (No: 2013M530412, 2016M602741) and Shuler-Foscue Endowment at Southern Methodist University. Some figures were prepared using the public domain Generic Mapping Tools GMT (Wessel and Smith, 1998).

References

Altamimi, Z., Collilieux, X., Legrand, J., et al., 2007. ITRF2005: a new release of the International Terrestrial Reference Frame based on time series of station positions and Earth Orientation Parameters. J. Geophys. Res. Sol. Earth 112 (B9), B9401.

Bai, D.H., Unsworth, M.J., Meju, M.A., et al., 2010. Crustal deformation of the eastern Tibtan plateau revealed by magnetotelluric imaging. Nat. Geosci. 3 (5), 358–362.

Bi, L., He, H., Wei, Z., Shi, F., 2012. Fractal properties of landforms in the Ordos Block and surrounding areas. China Geomorphol. 175–176, 151–162.

Chang, X., Liu, Y.K., He, J.K., Sun, H.C., 2007. Lower velocities beneath the taihang mountains, northeastern China. Bull. Seismol. Soc. Am. 97, 1364–1369.

Chen, X.B., Zang, S.X., Liu, Y.G., Wei, R.Q., 2005. Horizontal movement of Ordos Block and the interaction of Ordos Block and adjacent blocks. J. Grad. School Chin. Acad. Sci. 22 (3), 309–314.

Chen, H., Ju, J.M., Wu, G.L., Shi, W., Ceng, Y.Y., Qu, H.J., 2015. Apatite fission-track thermochronological constraints on the pattern of late Mesozoic-Cenozoic uplift and exhumation of the Qinling Orogen, central China. J. Asian Earth Sci. 114, 649–673.

Cheng, B., Cheng, S.Y., Zhang, G.W., Zhao, D.P., 2014. Seismic structure of the helan-Liupan-Ordos western margin tectonic belt in north-Central China andits geodynamic implications. J. Asian Earth Sci. 87 (15), 141–156.

China Earthquake Administration (CEA), 1995. Historical Strong Earthquake Catalog of China (2300B.C.–1911A.D.). Earthquake Publishing House, Beijing, in Chinese.

China Earthquake Administration (CEA), 1999. Recent Earthquake Catalog of China (1912–1990A.D., MSZ4.7). Chinese Science and Technology Press, Beijing (in Chinese).

Cui, D.X., Hao, M., Li, Y.H., Wang, W.P., Qing, X.L., Li, C.J., 2016. Present-day crustal movement and strain of the surrounding area of Ordos block derived from repeated GPS observations. Chin. J. Geophys. 59 (10), 3646–3661 (in Chinese with English abstract).

Dai, W.Q., Ren, J., Zhao, X.M., et al., 2004. Characteristics of horizontal crustal movement in Weihe basin and adjacent zones by GPS observation. Acta Seismol. Sin. 26 (3), 256–260 (in Chinese with English abstract).

Deng, Q., You, H., 1985. The tectonic activity and formation mechanism of the down-faulted basin around Ordos block. In: Institute of Geology, State Seismological Bureau of China (Ed.), Research on Recent Crustal Movement. Seismological Press, Beijing, pp. 58–78 (in Chinese).

Deng, J., Zhao, H., Mo, X., 1996. Root Structure of Chinese Continent-Key of Continental Dynamics. Geological Publishing House, Beijing (in Chinese).

Deng, Q., Zhang, P., Ran, Y., Yang, X., Min, W., Chu, Q., 2003. Basic characteristics of active tectonics of China. Sci. China Ser. D 46, 356–372.

Dong, D., Herring, T., King, R., 1998. Estimating regional deformation from a combination of space and terrestrial geodetic data. J. Geod. 72, 200–214.

Dong, D., Fang, P., Bock, Y., Webb, F., Prawirodirdjo, L., Kedar, S., Jamason, P., 2006. Spatiotemporal filtering using principal component analysis and Karhunen-Love expansion approaches for regional GPS network analysis. J. Geophys. Res. 111, B03405.

El-Fiky, G.S., Kato, T., Yoichiro, F.J., 1997. Distribution of vertical crustal movement rates in the Tohoku district, Japan, predicted by least-squares collocation. J. Geod. 71, 432–442.

England, P.C., Houseman, G.A., 1986. Finite strain calculations of continental deformation, 2, comparison with the India-Asia collision. J. Geophys. Res. 91, 3664–3676.

Fan, J.X., Ma, J., Gan, W.J., 2003. The motion integration and activity alternating of different orientation boundary of Ordos block. Sci. China Ser. D 33 (in Chinese) (Supplement).
Feng, X.J., Dai, W.Q., 2004. Lateral migration of fault activity in Weihe basin. Acta Seismol. Sin. 26 (2), 174–182 (in Chinese with English abstract).
Fu, R.S., Huang, J.H., 2001. Geodynamics. Higher Education Press, Beijing (in Chinese).
Gan, W.J., Zhang, P.Z., Shen, Z.K., Niu, Z.J., Wang, M., Wan, Y.G., Zhou, D.M., Cheng, J., 2007. Present-day crustal motion within the Tibetan Plateau inferred from GPS measurements. J. Geophys. Res. 112, B08416.
Gao, G.M., Kang, G.F., Li, G.Q., Bai, C.H., 2015. Crustal magnetic anomaly in the Ordos region and its tectonic implications. J. Asian Earth Sci. 109, 63–73.
Guo, Z., Chen, J.Y., 2016. Crustal structure of the eastern Qinling orogenic belt and implication for reactivation since the Cretaceous. Tectonophysics 683, 1–11.
Guo, L.Q., Zhan, W., Yang, G.H., Bo, W.J., 2010. Short-term displacement and characteristics of strain rate of Shanxi fault subsidence zone. 30 (4): 37–42. (in Chinese with English abstract).
Heiskanen, W.A., Moritz, H., 1967. Physical Geodesy. W.H Freeman and Co. Ltd., San Francisco, CA.
Herring, T.A., 2002. GLOBK: Global Kalman Filter VLBI and GPS Analysis Program Version 10.0. Massachusetts Institute of Technology, Cambridge.
Hu, B., Zhu, Y.Q., Jiang, Z.S., 2006. Vertical crustal deformation field in the Guanzhong area and its dynamic evolution characteristics, J. Seismol. Res., 29 (2): 151–156 (in Chinese with English abstract).
Hu, Bin, Zhu, Yiqin, Tian, Qinjian, et al., 2006b. Study on gravity field and its dynamic evolutional characteristics in the guanzhong area. Earthq. Res. China 22 (2), 172–181 (in Chinese with English abstract).
Huang, J.L., Zhao, D.P., 2006. High-resolution mantle tomography of China and surrounding regions. J. Geophys. Res. Solid Earth 111 (B9).
Jiang, Z.S., Liu, J.N., 2010. The method in establishing strain field and velocity field of crustal movement using least squares collocation. Chin. J. Geophys. 53 (5), 1109–1117 (in Chinese with an English abstract).
Jiang, W., Hao, T., Song, H., 2000a. Crustal structure and geological and geophysical features of Ordos basin. Prog. Geophys. 15, 45–53 (in Chinese with English Abstract).
Jiang, W.L., Xiao, Z.M., Xie, X.S., 2000b. Segmentations of active normal dip-slip faults around Ordos block according to their surface ruptures in historical strong earthquakes. Earthq. Sci. 13 (5), 552–562.
Jiang, Z.S., Ding, P., Wang, S.X., et al., 2001. Telluruc Deformation Monitoring and Earthquake Predicetion in West China. Seismological Press, Beijing, pp. 7–27 (in Chinese).
Jiang, Z.S., Zhang, X., Zhu, Y.Q., Wang, X.L., Zhang, S.X., 2003. Regional tectonic deformation background before Ms 8.1 earthquake on the west of Kunlun Mountain pass. Sci. China Ser. D 33 (B04), 163–172 (in Chinese with an English abstract).
Jiang, G.Y., Xu, C.J., Wen, Y.M., Xu, X.W., Ding, K.H., Wang, J.J., 2014. Contemporary tectonic stressing rates of major strike-slip faults in the Tibetan Plateau from GPS observations using Least-Squares Collocation. Tectonophysics 615–616, 85–95.
Jin, H.L., Hu, X.K., Wang, Y.B., 2012. Study on strain field around Zhangjiakou-Bohai seismic belt with least-square collocation, J. Geodesy Geodyn., 32 (2): 7–10 (in Chinese with an English abstract).
King, R.W., Bock, Y., 2000. Documentation for the GAMIT GPS Analysis Software Release 10.0. Massachusetts Institute of Technology, Cambridge.
Li, Z.H., Liu, B.J., Yuan, H.K., et al., 2014. Fine crustal structure and tectonics of Linfen Basin-from the results of seismic reflection profile. Chin. J. Geophys. 57 (5), 1487–1497 (in Chinese with English abstract).
Li, B., Mathilde, B.S., Kuvvet, A., 2015. Coulomb stress evolution in the Shanxi rift system, North China, since 1303 associated with coseismic, post-seismic and interseismic deformation. Geophys. J. Int. 203, 1642–1664.
Lin, A., Rao, G., Yan, B., 2015. Flexural fold structures and active faults in the northern-western Weihe Graben, Central China. J. Asian Earth Sci. 114, 226–241.
Liu, M., Cui, X., Liu, F., 2004. Cenozoic rifting and volcanism in eastern China: a mantle dynamic link to the Indo-Asian collision. Tectonophysics 393, 29–42.
Liu, M., Yang, Y.Q., Shen, Z., Wang, S., Wang, M., Wan, Y., 2007. Active tectonics and intra-continental earthquakes in China: the kinematics and geodynamics. In: Stein, S., Mazzotti, S. (Eds.), Continental Intraplate Earthquakes: Science, Hazard, and Policy Issues, vol. 425. Geological Society of America Special Paper, pp. 299–318.
Liu, J.W., Xie, F.R., Lv, Y.J., 2016. Seismic hazard assessments for the Ordos Block and its periphery in China. Soil Dyn. Earthq. Eng. 84, 70–82.
Yu, Z.C., Lu, L.C., 1978. The Foundation of Survey Adjustment. Surveying and Mapping Publisher, Beijing (in Chinese).
Meng, Q., Zhang, G., 2000. Geologic framework and tectonic evolution of the Qinling orogen, central China. Tectonophysics 323, 183–196.
Molnar, P., Deng, Q., 1984. Faulting associated with large earthquakes and the average rate of deformation in central and eastern Asia. J. Geophys. Res. 89, 6203–6227.
Molnar, P., Lyon-Caent, H., 1989. Fault plane solutions of earthquakes and active tectonics of the Tibetan Plateau and its margins. Geophys. J. Int. 99, 123–154.
Moritz, H., High physics Geodetic Survey (in Chinese). Ning, J.S., et al., 1984.Trans. Beijing: Surveying and Mapping Press, 50-125.
Myers, J.R., Gomez, F.G., 2010. Analysis of Subsidence and Ground Fissuring in the FenWei Basin (Northern China) using Radar Interferometry. AGU Fall Meeting Abstracts#H23F-1297.
Pan, S., Niu, F., 2011. Large contrasts in crustal structure and composition between the Ordos plateau and the NE Tibetan plateau from receiver function analysis. Earth Plan. Sci. Lett. 303, 291–298.
Qu, W., Lu, Z., Zhang, Q., Peng, J.B., Wang, Q.L., Jane, D., Zhang, M., 2014a. Kinematic model of crustal deformation of fenwei basin: China based on GPS observations. J. Geodyn. 75, 1–8.
Qu, F.F., Zhang, Q., Lu, Z., Zhao, C.Y., Yang, C.S., Zhang, J., et al., 2014b. Land subsidence and ground fissures in Xi'an China 2005–2012 revealed by multi-band InSAR time-series analysis. Remote Sens. Environ. 155, 366–376.
Rao, G., Lin, A., Yan, B., Jia, D., Wu, X.J., 2014. Tectonic activity and structural features of active intracontinental normal faults in the Weihe Graben central China. Tectonophysics 636, 270–285.
Rao, G., Lin, A., Yan, B., 2015. Paleoseismic study on active normal faults in the southeastern Weihe Graben, central China. J. Asian Earth Sci. 114, 212–225.
Ratschbacher, L., Hacker, B., Calvert, A., Webb, L., Grimmer, J., McWilliams, M., Ireland, T., Dong, S., Hu, J., 2003. Tectonics of the Qinling (Central China): tectonostratigraphy, geochronology, and deformation history. Tectonophysics 366, 1–53.
Ren, J., Peng, J.B., Wang, F.Y., et al., 2012. The research of deep structural features of Weihe basin and adjacent areas. Chin. J. Geophys. 55 (9), 2939–2947 (in Chinese with English abstract).
Riguzzi, F., Crespi, M., Devoti, R., Doglioni, C., Pietrantonio, G., Pisani, A.R., 2012. Geodetic strain rate and earthquake size: new clues for seismic hazardstudies. Phys. Earth Plan. Int. 206–207, 67–75.
Segall, P., 2010. Earthquake and Volcano Deformation. Princeton University Press, New Jersey/Oxfordshire.
Shaanxi Earthquake Information Network (SEIN), 2011. Historical Earthquakes in Shaanxi Province (Accessed 30.08.14) (in Chinese) http://www.eqsn.gov.cn/manage/html/8abd83af1c88b3f2011c88b74299001f/sxlsdz/index.html.
Shen, Z.K., Zhao, C.K., Yin, A., Li, Y.X., David, D.J., Fang, P., Dong, D.N., 2000. Contemporary crustal deformation in east Asia constrained by Global Positioning System measurements. J. Geophys. Res.: Solid Earth 105 (B3), 5721–5734.
Shi, Y.L., Zhu, S.B., 2006. Discussion on method of calculating strain with GPS displacement date. J. Geod. Geodyn. 26 (1), 1–8 (in Chinese with an English abstract).
Shi, Y.Q., Feng, X.J., Dai, W.Q., Li, X.N., Ren, J., Zhong, J., 2008. Geometric structure and formation mechanism of Lintong2Chang'an fault zone. Acta Seismol. Sin. 30 (2), 152–164 (in Chinese with English abstract).
Song, M.Q., Zheng, Y., Ge, C., et al., 2012. Relocation of small to moderate earthquake in Shanxi province and its relation to the seismogenic structures. Chin. J. Geophys. 55 (2), 513–525 (in Chinese with English abstract).
State Seismological Bureau Research Group (SSBRG), 1988. Active Fault System Around the Ordos, 335. Seismological Press, Beijing, China (in Chinese).
Sun, Y., Dong, S., Zhang, H., Shi, Y., 2014. Numerical investigation of the geodynamic mechanism for the late Jurassic deformation of the Ordos block and surrounding orogenic belts. J. Asian Earth Sci. 114 (4), 623–633.
Sun, Y.J., Dong, S.W., Zhang, H.A., Shi, Y.L., 2015. Numerical investigation of the geodynamic mechanism for the late Jurassic deformation of the Ordos block and surrounding orogenic belts, J. Asian Earth Sci., 623–633.
Ta, L., Chen, F.C., Zhou, H.T., Guo, B.Z., Guo, L.Q., 2014. Study on modern crustal vertical motion in Shanxi area, J. Geodesy Geodyn. 34 (1): 32–37 (in Chinese with English abstract).
Tang, Y.C., Chen, Y.J., Fu, Y.V., Wang, H., Zhou, S., Sandvol, E., Ning, J.Y., Feng, Y.G., Liu, M., 2010. Mantle anisotropy across the southwestern boundary of the Ordos block. North China. Earthq. Sci. 23 (6), 549–553.
Tian, Z.Y., Han, P., Xu, K.D., 1992. The Mesozoic—Conozic east China rift system. Tectonophysics 208, 341–363.
Tian, X., Teng, J., Zhang, H., Zhang, Z., Zhang, Y., Yang, H., Zhang, K., 2011. Structure of crust and upper mantle beneath the Ordos Block and the Yinshan Mountains revealed by receiver function analysis. Phys. Earth Plan. In. 184, 186–193.
Turcotte, D.L., Schubert, G., 1982. Geodynamics. University Press, Cambridge.
Wang, K.Y., Ma, J., Diao, G.L., 2012. Presentday stress state of the Shanxi tectonic belt. Geodyn. Tectonophys. 3 (3), 195–202.
Wang, S.X., Jiang, F.Y., Hao, M., et al., 2013. Investigation of features of present 3D crustal movement in eastern edge of Tibet plateau. Chin. J. Geophys. 56 (10), 3334–3345 (in Chinese with an English abstract).
Wang, Z.T., Zhou, H.R., Wang, X.L., Jing, X.C., 2015. Characteristics of the crystalline basement beneath the Ordos Basin: constraint from aeromagnetic data. Geosci. Front. 6, 465–475.
Wang, M., 2009. Analysis of GPS Data with High Precision and Study on Present-Day Crustal Deformation in China (Doctoral Thesis). Institute of Geology, China Earthquake Administration (in Chinese).
Ward, S.N., 1994. A multidisciplinary approach to seismic hazard in southern California. Bull. Seismol. Soc Am. 84 (5), 1293–1309.
Wesnousky, S.G., Jones, L.M., Scholz, C.H., Deng, Q., 1984. Historic seismicity and rates of crustal deformation along the margins of the Ordos block, north China. Bull. Seism. Soc. Am. 74, 1767–1783.
White, L.T., Lister, G.S., 2012. The collision of India with Asia. J. Geodyn. 56–57, 7–17.
Wu, J.C., Tang, H.W., Chen, Y.Q., Li, Y.X., 2006. The current strain distribution in the North China Basin of eastern China by least-squares collocation. J. Geodyn. 41, 462–470.
Wu, Y.Q., Jiang, Z.S., Yang, G.H., Wei, W.X., Liu, X.X., 2009. The application and method of GPS strain calculation in whole mode using least-squares

collocation in spheresurface. Chin. J. Geophys. 52 (7), 1707–1711 (in Chinese with an English abstract).
Wu, Y.Q., Jiang, Z.S., Yang, G.H., Wei, W.X., Liu, X.X., 2011. Comparison of GPS strain rate computing methods and their reliability. Geophys. J. Int. 185, 703–717.
Wu, Y.Q., Jiang, Z.S., Zhao, J., Liu, X.X., Wei, W.X., Liu, Q., Li, Q., Zou, Z.Y., Zhang, L., 2015. Crustal deformation before the 2008 Wenchuan Ms8.0 earthquake studied using GPS data. J. Geodyn. 85, 11–23.
Xu, X.W., Ma, X.Y., 1992. Geodynamics of the Shanxi rift system China. Tectonophysics 208, 325–340.
Xu, Y., 2006. Using basalt geochemistry to constrain Mesozoic-Cenozoic evolution of the lithosphere beneath North China Craton. Front. Earth Sci. 13, 93–104 (in Chinese with English Abstract).
Yang, G.H., et al., 2000. The movement trend and dynamic character in Shanxi fault zone. Earthq. Res. China 18 (2), 148–156 (in Chinese with English abstract).
Yang, J.H., Wu, F.Y., Wilde, S.A., Belousova, E., Griffin, W.L., 2008. Mesozoic decratonization of the north China block. Geology 36, 467–470.
Yang, M.H., Li, L., Zhou, J., Qu, X.Y., Zhou, D., 2013. Segmentation and inversion of the Hangjinqi fault zone, the northern Ordos basin (North China). J. Asian Earth Sci. 70 (71), 64–78.
Ye, H., Shedlock, K.M., Hellinger, S.J., Sclater, J.G., 1985. The North China Basin: an example of a Cenozoic rifted intraplate basin. Tectonics 4, 153–169.
Yuan, T., Feng, X., 2010. The 1556 Huaxian Great Earthquake. Seismological Press, Beijing, pp. 386 (in Chinese).
Zhang, X., Jiang, Z.S., Zhang, S.X., 1998a. Whole calculation of the crustal visual strain field with the least square collocation. Crust. Deform. Earthq. 18 (2), 57–62 (in Chinese with an English abstract).
Zhang, Y.Q., Mercier, J.L., Vergely, P., 1998b. Extension in the graben systems around the Ordos (China), and its contribution to the extrusion tectonics of south China with respect to Gobi-Mongolia. Tectonophysics 285, 41–75.
Zhang, Y.Q., Ma, Y.S., Yang, N., Shi, W., Dong, S.W., 2003. Cenozoic extensional stress evolution in North China. J. Geodyn. 36 (5), 591–661.
Zhang, P.Z., Gan, W.J., Shen, Z.K., 2005. A coupling model of rigid-block movement and continuous deformation: patterns of the present-day deformation of China's continent and its vicinity. Acta Geol. Sin. 79 (6), 748–756.
Zhang, X., Jiang, F.Y., Tang, H.T., Li, R.S., Jia, P., 2011. Analysis on the section deformation and strain accumulation of the Fen-Wei fracture belt observed by GPS in recent 10 years, J. Seismol. Res., 34(4): 504–510 (in Chinese with English abstract).
Zhang, Q., Qu, W., Wang, Q.L., Peng, J.B., Drummond, J., Li, Z.H., Lin, Q., 2011b. Analysis of present tectonic stress and regional ground fissure formation mechanism of the Weihe Basin. Surv. Rev. 43 (322), 382–389.
Zhang, J., Wu, Y.Q., Liu, Q., Chen, R.H., 2013. Relationship between plane strain rate gradient of GPS horizontal deformation and strong earthquake risk area. Acta Seismol. Sin. 35 (6), 828–835 (in Chinese with an English abstract).